AIAA JOURNAL
Vol. 36, No. 2, February 1998

Improved Time-Dependent Flowfield Solution for Solid Rocket Motors

J. Majdalani*
Marquette University, Milwaukee, Wisconsin 53233
and
W. K. Van Moorhem†
University of Utah, Salt Lake City, Utah 84112

A model of the time-dependent velocity field in solid rocket motors is derived analytically for an oscillatory field that is subject to steady sidewall injection. The oscillatory pressure amplitude is assumed to be small by comparison to the mean pressure. The mathematical approach includes solving the momentum equation governing the rotational flow using separation of variables and multiple scales. This requires identifying scales at which unsteady inertia, convection, and diffusion are significant. A composite scale is obtained that combines three disparate scales. The time-dependent axisymmetric solution obtained incorporates the effects of unsteady inertia, viscous diffusion, and the radial and axial convection of unsteady vorticity by Culick's mean flow components (Culick, F. E. C., "Rotational Axisymmetric Mean Flow and Damping of Acoustic Waves in a Solid Propellant Rocket," *AIAA Journal*, Vol. 4, No. 8, 1966, pp. 1462–1464). The resulting agreement with the numerical solution to the momentum equation is remarkable. The uncertainty in a short analytical expression is found to be smaller than the injection Mach number, which represents the error associated with the mathematical model itself. The multiple-scales solution agrees extremely well with Flandro's recent flowfield solution (Flandro, G. A., "On Flow Turning," AIAA Paper 95-2730, July 1995). The present solution has the advantage of being shorter, more manageable in extracting quantities of interest, and capable of showing the significance of physical parameters on the solution.

Nomenclature

A_p	= dimensional oscillatory pressure amplitude
a_0	= mean stagnation sound speed, $\sqrt{(\gamma p_0/\rho_0)}$
k_m	= wave number; $m\pi R/L = \omega_0 R/a_0$
L	= internal chamber length
M_b	= wall injection Mach number, V_b/a_0
p	= dimensionless pressure, p^*/p_0
p_0	= mean chamber pressure, $\rho_0 a_0^2/\gamma$
R	= dimensional effective radius
Re_k	= kinetic Reynolds number; $\omega_0 R^2/\nu_0 = k_m/\delta^2$
r	= radial position; $r^*/R = (1-y)$
r_1	= modified scale in multiple-scales procedures
S_p	= penetration number; $V_b^3\omega_0^{-2}\nu_0^{-1}R^{-1} = M_b^3 k_m^{-2}\delta^{-2}$
Sr	= Strouhal number; $\omega_0 R/V_b = k_m/M_b$
t	= dimensionless time; $t^* a_0/R = \bar{t}/k_m$
$\bar{t}$	= dimensionless time; $k_m t = 2\pi f_m t^*$
U	= Culick's[12] mean flow velocity, (U_r, U_z)
U_r	= radial mean flow velocity, $-r^{-1}\sin\theta$
U_z	= axial mean flow velocity, $\pi z\cos\theta$
$\hat{u}$	= dimensionless acoustic velocity, $\hat{u}^*/a_0$
$\tilde{u}$	= dimensionless vortical velocity, $\tilde{u}^*/a_0$
$u^{(1)}$	= total unsteady velocity; $u^{*(1)}/a_0 = (\hat{u}+\tilde{u})$
V_b	= radial injection speed at the wall
y	= distance from the wall; $y^*/R = (1-r)$
z	= axial distance from the head end, z^*/R
γ	= mean ratio of specific heats
δ_s	= Stokes' characteristic thickness, $\sqrt{(\nu_0/\omega_0)}$
δ^2	= inverse of Re; $\nu_0/(a_0 R) = 1/Re$
ε	= small parameter; $Re_k^{-1} = \delta_s^2/R^2$
ε_w	= pressure wave amplitude, A_p/p_0
θ	= characteristic variable, $\pi r^2/2$
λ_n	= separation constant ($2n+1$, where n is 0, 1, ...)
ν_0	= chamber fluid mean kinematic viscosity
ξ	= viscous parameter; $S_p^{-1} = k_m^2\delta^2/M_b^3$
ρ_0	= chamber mean density
ω_m	= dimensionless circular frequency, $m\pi R/L$
ω_0	= dimensional circular frequency, $m\pi a_0/L$

Subscripts

r, z	= radial or axial component
$0, 1, \ldots$	= order of approximation

Superscripts

$(0), (1), \ldots$	= perturbation level
$*$	= dimensional quantity
$\hat{}$	= acoustic oscillations
$\tilde{}$	= vortical oscillations

Introduction

THE time-dependent velocity field plays an essential role in the accurate prediction of combustion instability in solid rocket motors. This is due to the mathematical nature of the stability integrals whose reliability depends on a precise representation of the velocity field.[1] This has instigated a number of researchers to investigate the true nature of the velocity field to improve the predictive capability of combustion stability programs. With such a goal in mind, Shaeffer and Brown[2] designed an elegant experiment to study the character of an oscillatory flow including sidewall injection of nitrogen through fine sintered bronze walls. Vuillot and Avalon,[3] Smith et al.,[4] Flandro and Roach,[5] and Sabnis et al.[6] made good use of various computational tools to study and explain the nature of the internal flowfield. Recent theoretical and computational studies of the transient evolution of the velocity field prescribed by harmonic endwall[7] and sidewall[8] disturbances have also been undertaken. The aforementioned studies concurred that flow rotationality was a

Received May 22, 1997; presented as Paper 97-2717 at the AIAA/ASME/SAE/ASEE 33rd Joint Propulsion Conference, Seattle, WA, July 6–9, 1997; revision received Sept. 13, 1997; accepted for publication Oct. 6, 1997.

*Assistant Professor, Department of Mechanical and Industrial Engineering. Member AIAA.
†Professor, Department of Mechanical Engineering. Senior Member AIAA.

significant element that must be accounted for to improve the widely used one-dimensional acoustic model employed, for example, in the standard stability prediction code of Nickerson et al.[9]

Credit must be given to Flandro,[10] who was among the earliest investigators to realize that the simple one-dimensional irrotational solution used to model the time-dependent field did not incorporate the effects of three dimensionality, mean flow interaction, convection of vorticity, and viscous diffusion, which could play significant roles in the prediction of combustion stability. Therefore, he attempted to solve the momentum equation governing the rotational time-dependent flowfield analytically. Because of the mathematical complexities, Flandro[10,11] realized at first that some terms needed to be sacrificed and others approximated to extract useful analytical solutions. His first approach[11] retained the radial convection of vorticity and viscous diffusion while ignoring the axial convection of vorticity. To solve the resulting equation exactly, Culick's[12] radial mean flow component had to be approximated to its constant value at the wall. The resulting solution provided much insight despite its limitation of being axially independent and applicable to a narrow region near the wall. As an improvement on Flandro's first solution,[11] the authors[13,14] employed multiple-scales expansions[15,16] to extract an axially independent analytical expression that utilized the exact mean flow profile. As a result, its applicability was not limited to a thin region near the wall as with the previous solution. However, it was limited in that it did not incorporate the axial dependence. In his second attempt, Flandro[17] neglected viscous diffusion and retained both radial and axial convection terms representing the transport of unsteady vorticity by Culick's mean flow component.[12] The resulting solution incorporated an axial dependence despite its limitation of being inviscid. Finally, in his third approach, Flandro[18] extracted a rotational and viscous solution that incorporated all of the important mechanisms. The last two approaches used regular perturbations and the vorticity equation. In the process, velocity was derived from vorticity, which was determined first. Flandro's last solution was very accurate because it depended on a perturbation parameter that is very small in rocket motors. The only undesirable feature of Flandro's last solution[18] is that it resulted in a rather complicated expression that did not show readily how the solution depended on the various parameters involved.

In the following analysis, a multiple-scales procedure will be employed to derive the time-dependent axisymmetric velocity field directly from the momentum equation. Beginning with the full momentum equation, a perturbation solution is obtained to the order of the Mach number. The uniformly valid solution will be shown to be very accurate, matching the numerical solution everywhere. Its advantage relative to previous models is that it is short, accurate, capable of indicating the role of various physical parameters, and incorporates all of the intricate physical mechanisms involved in the problem, including the axial dependence.

Analysis

Reminiscent of a previously used approach,[14] the analysis will follow typical assumptions employed when modeling the internal flowfield in rocket motors. In the process, the total velocity is separated into two parts, $\boldsymbol{u} = M_b\boldsymbol{U} + \boldsymbol{u}^{(1)}$: 1) a steady flow component ($M_b\boldsymbol{U}$) given by Culick's profile[12] and 2) a time-dependent component $\boldsymbol{u}^{(1)}$ that we propose to find.

Fundamental Equations

The first-order time-dependent motion is governed by the viscous momentum equation[10,17]

$$\frac{\partial \boldsymbol{u}^{(1)}}{\partial t} + M_b\left[\nabla\left(\boldsymbol{u}^{(1)}\cdot\boldsymbol{U}\right) - \boldsymbol{u}^{(1)}\times(\nabla\times\boldsymbol{U}) - \boldsymbol{U}\times\left(\nabla\times\boldsymbol{u}^{(1)}\right)\right] = \delta^2\left[\frac{4}{3}\nabla\left(\nabla\cdot\boldsymbol{u}^{(1)}\right) - \nabla\times\left(\nabla\times\boldsymbol{u}^{(1)}\right)\right] - \frac{\nabla p^{(1)}}{\gamma} \tag{1}$$

The total unsteady velocity vector can be broken up into acoustic (compressible, inviscid, irrotational) and solenoidal (incompressible, viscous, rotational) parts

$$\boldsymbol{u}^{(1)} = \hat{\boldsymbol{u}} + \tilde{\boldsymbol{u}} \tag{2}$$

Substituting Eq. (2) into Eq. (1), two equations result:

$$\frac{\partial \hat{\boldsymbol{u}}}{\partial t} = -\frac{\nabla \hat{p}}{\gamma} - M_b[\nabla(\hat{\boldsymbol{u}}\cdot\boldsymbol{U}) - \hat{\boldsymbol{u}}\times(\nabla\times\boldsymbol{U})] + \frac{4}{3}\delta^2\nabla(\nabla\cdot\hat{\boldsymbol{u}}) \tag{3}$$

$$\frac{\partial \tilde{\boldsymbol{u}}}{\partial t} + M_b[\nabla(\tilde{\boldsymbol{u}}\cdot\boldsymbol{U}) - \tilde{\boldsymbol{u}}\times(\nabla\times\boldsymbol{U}) - \boldsymbol{U}\times(\nabla\times\tilde{\boldsymbol{u}})] = \delta^2[\nabla\times(\nabla\times\tilde{\boldsymbol{u}})] \tag{4}$$

Equation (3) yields the first-order acoustic term $\hat{\boldsymbol{u}}$ that is given by the plane wave solution[5,11,17]

$$\hat{\boldsymbol{u}}(z,t) = i(\varepsilon_w/\gamma)\sin(k_m z)\exp(-ik_m t)\boldsymbol{e}_z \tag{5}$$

$$\hat{p}(z,t) = \varepsilon_w\cos(k_m z)\exp(-ik_m t) \tag{6}$$

Equation (4), which we propose to solve, governs the rotational component $\tilde{\boldsymbol{u}}$, where

$$\tilde{\boldsymbol{u}} = \tilde{u}_r\boldsymbol{e}_r + \tilde{u}_z\boldsymbol{e}_z \tag{7}$$

Unsteady Rotational Momentum Equation

When Eq. (7) is substituted back into Eq. (4), the radial and axial components of the rotational momentum equation are obtained:

$$\frac{\partial \tilde{u}_r}{\partial t} = -M_b\left[\frac{\partial}{\partial r}(\tilde{u}_r U_r) + U_z\frac{\partial \tilde{u}_r}{\partial z} + \tilde{u}_z\frac{\partial U_r}{\partial z}\right] + \frac{\delta^2}{r}\frac{\partial}{\partial z}\left[r\left(\frac{\partial \tilde{u}_r}{\partial z} - \frac{\partial \tilde{u}_z}{\partial r}\right)\right] \tag{8}$$

$$\frac{\partial \tilde{u}_z}{\partial t} = -M_b\left[\frac{\partial}{\partial z}(\tilde{u}_z U_z) + U_r\frac{\partial \tilde{u}_z}{\partial r} + \tilde{u}_r\frac{\partial U_z}{\partial r}\right] + \delta^2\left(\frac{\partial^2 \tilde{u}_z}{\partial r^2} + \frac{1}{r}\frac{\partial \tilde{u}_z}{\partial r} - \frac{1}{r}\frac{\partial \tilde{u}_r}{\partial z} - \frac{\partial^2 \tilde{u}_r}{\partial r\,\partial z}\right) \tag{9}$$

Subject to later theoretical verification, the magnitude of $\tilde{u}_r/\tilde{u}_z$ is assumed to be of order M_b. Full numerical solutions and experimental measurements of the radial component also support this notion.[2–6] Being a small quantity, ignoring this component at the first perturbation expansion level of the rotational velocity will not affect the solution, which is only accurate to the first order in the Mach number. Dropping $\tilde{u}_r$ from Eq. (9), the rotational momentum equation governing the axial velocity component $\tilde{u}_z$ becomes

$$\frac{\partial \tilde{u}_z}{\partial t} = -M_b\left[\frac{\partial}{\partial z}(\tilde{u}_z U_z) + U_r\frac{\partial \tilde{u}_z}{\partial r}\right] + \delta^2\left(\frac{\partial^2 \tilde{u}_z}{\partial r^2} + \frac{1}{r}\frac{\partial \tilde{u}_z}{\partial r}\right) \tag{10}$$

Solution by Separation of Variables

Letting $\tilde{u}_z = \bar{u}_z(r,z)\exp(-ik_m t)$, Eq. (10) becomes

$$ik_m\bar{u}_z(r,z) = M_b\left[\frac{\partial}{\partial z}(\bar{u}_z U_z) + U_r\frac{\partial \bar{u}_z}{\partial r}\right] - \frac{\delta^2}{r}\frac{\partial}{\partial r}\left(r\frac{\partial \bar{u}_z}{\partial r}\right) \tag{11}$$

Rearranging Eq. (11) and expressing the resulting constants in terms of the nondimensional Strouhal and kinetic Reynolds numbers, the result is

$$i\bar{u}_z(r,z) = \frac{1}{Sr}\left[\bar{u}_z\frac{\partial U_z}{\partial z} + U_z\frac{\partial \bar{u}_z}{\partial z} + U_r\frac{\partial \bar{u}_r}{\partial r}\right] - \frac{1}{Re_k}\left(\frac{\partial^2 \bar{u}_z}{\partial r^2} + \frac{1}{r}\frac{\partial \bar{u}_z}{\partial r}\right) \tag{12}$$

Substituting Culick's steady flow velocity,[12] using ε instead of the inverse of Re_k, and rearranging so that z-dependent terms are isolated, one gets

$$z\frac{\partial \bar{u}_z}{\partial z} = \frac{Sr}{\pi}\sec\left(\frac{\pi}{2}r^2\right)\left\{\left[i - \frac{\pi}{Sr}\cos\left(\frac{\pi}{2}r^2\right)\right]\bar{u}_z + \frac{1}{rSr}\sin\left(\frac{\pi}{2}r^2\right)\frac{\partial \bar{u}_z}{\partial r} + \varepsilon\left(\frac{\partial^2 \bar{u}_z}{\partial r^2} + \frac{1}{r}\frac{\partial \bar{u}_z}{\partial r}\right)\right\} \tag{13}$$

Equation (13) suggests using separation of variables to investigate a solution of the form

$$\bar{u}_z(r, z) = V(r)Z(z) \tag{14}$$

Substituting Eq. (14) into Eq. (13) and rearranging to show that terms that are purely functions of r or z can be isolated, Eq. (13) becomes

$$\frac{z}{Z}\frac{dZ}{dz} = \frac{Sr}{\pi V}\sec\left(\frac{\pi}{2}r^2\right)\left\{\left[i - \frac{\pi}{Sr}\cos\left(\frac{\pi}{2}r^2\right)\right]V + \frac{1}{rSr}\sin\left(\frac{\pi}{2}r^2\right)\frac{dV}{dr} + \frac{\varepsilon}{r}\frac{d}{dr}\left(r\frac{dV}{dr}\right)\right\} = \lambda_n \tag{15}$$

where it can be easily shown that the separation constant λ_n must be strictly positive for a physically acceptable solution. For every value of the eigenvalue λ_n, a solution to the axially dependent and radially dependent eigenfunctions $Z_n(z)$ and $V_n(r)$ must be obtained. Integration of the axially dependent equation is straightforward. The exact result is

$$\frac{dZ_n}{dz} - \frac{\lambda_n}{z}Z_n = 0 \Rightarrow Z_n(z) = c_n z^{\lambda_n} \tag{16}$$

where c_n is an integration constant corresponding to a given value of the separation eigenvalue. Because the governing equation is linear, any linear combination of two or more solutions, corresponding to two or more separation constants, is also a solution. Therefore, one can write, in general, for all possible eigenvalues λ_n,

$$\bar{u}_z(r, z) = \sum_{\lambda_n} c_n z^{\lambda_n} V_n(r) \tag{17}$$

where λ_n is to be determined from the no-slip boundary condition at the wall. This is achieved when, at the wall, the rotational and irrotational components of the time-dependent velocity cancel out:

$$\boldsymbol{u}^{(1)} = \boldsymbol{0} \qquad \text{or} \qquad \bar{u}_z = -\hat{u}_z \tag{18}$$

which translates into

$$\bar{u}_z \exp(-ik_m t) = -(\varepsilon_w/\gamma)i \sin(k_m z)\exp(-ik_m t) \tag{19}$$

$$\Rightarrow \bar{u}_z|_{r=1} = -(\varepsilon_w/\gamma)i \sin(k_m z) \tag{20}$$

Inserting Eq. (20) into Eq. (17) and writing out the MacLaurin series expansion for the sine function, the following equality must be true:

$$\sum_{\lambda_n} c_n z^{\lambda_n} V_n\Big|_{r=1} = -\frac{\varepsilon_w}{\gamma}i\sum_{n=0}^{\infty}\frac{(-1)^n(k_m z)^{2n+1}}{(2n+1)!} \tag{21}$$

Clearly, the left- and right-hand sides of Eq. (21) will be identical when

$$\lambda_n = 2n + 1, \qquad n = 0, 1, 2, \ldots \tag{22}$$

$$c_n = -\frac{\varepsilon_w}{\gamma}i\frac{(-1)^n(k_m)^{2n+1}}{(2n+1)!} \tag{23}$$

$$V_n(1) = 1 \tag{24}$$

Substituting back Eqs. (22) and (23), Eq. (17) becomes

$$\bar{u}_z(r, z) = -\frac{\varepsilon_w}{\gamma}i\sum_{n=0}^{\infty}\frac{(-1)^n(k_m z)^{2n+1}}{(2n+1)!}V_n(r) \tag{25}$$

The velocity eigenfunction V_n is left to be determined from the separable, radially dependent part of Eq. (15):

$$\varepsilon\left(\frac{d^2V_n}{dr^2} + \frac{1}{r}\frac{dV_n}{dr}\right) + \frac{1}{rSr}\sin\left(\frac{\pi}{2}r^2\right)\frac{dV_n}{dr} + \left[i - \frac{\pi}{Sr}(1+\lambda_n)\cos\left(\frac{\pi}{2}r^2\right)\right]V_n = 0 \tag{26}$$

which is subject to the following two boundary conditions.

No-slip at the wall:

$$V_n|_{r=1} = 1 \tag{27}$$

Centerline symmetry:

$$\left.\frac{dV_n}{dr}\right|_{r=0} = 0 \tag{28}$$

Radially Dependent Velocity Function

Integration of Eq. (26) is not straightforward. The inherent difficulty in analytically integrating this second-order ordinary differential equation (ODE) stems from the existing variable coefficients, which, unless linearized, do not appear to permit an exact solution. This impediment is behind the multiple formulations of one-dimensional,[11,13,14] two-dimensional inviscid,[17] and two-dimensional viscous,[18] models, whose purpose was, in reality, to overcome this mathematical obstacle using different levels of approximations. As will be shown, this difficulty can be circumvented by the multiple-scales approach, provided that the proper characteristic scales are known. The multiple-scales technique will be capable of integrating the radially dependent momentum equation to a relatively high degree of accuracy, theoretically, to the order of ε, which is more than sufficiently accurate because ε is always much smaller than M_b.

Multiple-Scales Procedure

The key issue for this method to work is a prior knowledge of the location and form of the characteristic scales. To that end, the first step will be to determine the local coordinate transformation(s) that can be associated with the particular phenomena that dominate in specific regions of interest.

Characteristic Scales

Mathematically, the characteristic scales are those that are capable of providing a balance in the governing equation between terms representing the interacting phenomena that are appreciable in a given region. Physically, they represent the scale at which order the momentum exchange between dominating phenomena, such as convection, diffusion, or inertia, takes place in reality. As will be demonstrated, four distinct regions with known characteristic scales are identified. Three of them correspond to the near-wall, centerline, and buffer regions. Both centerline and buffer regions are characterized by similar magnified scales and occur in a zone that is far from the solid boundary. The near-wall region, which is highly rotational, is characterized by a compressed scale. Between the two zones, a transition zone exists where all existing physical phenomena are in balance. This region is characterized by a base scale that is neither stretched nor compressed, corresponding to the unmodified spatial coordinate itself. In what follows, a systematic method that allows identifying each particular scale will be presented.

Near-Wall Scale

Near the wall, unsteady inertia and mean flow convection dominate. Changes in the oscillatory velocity in this region are slow, with almost constant amplitude. Instead of stretching the spatial coordinate near the wall, a compression of the coordinate is required here because the oscillatory amplitude decays slowly near the wall where the effect of blowing is appreciable. In compressing the spatial dimension, a transformation of the independent variable is needed. Introducing the near-wall transformation variable $r_1 = \varepsilon(1 - r)$, a balance between unsteady inertia and convection is achieved in Eq. (26) because the actual velocity gradient near the wall is always large[14]:

$$\frac{\varepsilon}{Sr}U_r\frac{dV_n}{dr_1} + \left[i - \frac{\pi}{Sr}(1+\lambda_n)\cos\left(\frac{\pi}{2}r^2\right)\right]V_n = -\varepsilon^3\left(\frac{d^2V_n}{dr_1^2} - \frac{1}{\varepsilon - r_1}\frac{dV_n}{dr_1}\right) \tag{29}$$

Centerline Scale

Approaching the centerline, blowing effects become negligible because the steady radial velocity becomes very small. The unsteady velocity amplitude approaches the acoustic amplitude. Instead of compressing the radial coordinate, a stretching or magnification of the scale is required here, because the wavelength, which is controlled by the mean flow velocity, becomes vanishingly small. Hence, an expansion of the region is required to account for small, yet rapid spatial changes in the oscillatory amplitude. Introducing the scale $r_1 = r^q \varepsilon^{-1}$ or its inverse $r_1 = \varepsilon r^{-q}$, a balance between unsteady inertia and diffusion can be achieved in Eq. (26):

$$q^2\varepsilon^{1-2/q}\left(r_1^{2(1+1/q)}\frac{\mathrm{d}^2V_n}{\mathrm{d}r_1^2}+r_1^{(1+2/q)}\frac{\mathrm{d}V_n}{\mathrm{d}r_1}\right)+\left[i-\frac{\pi}{Sr}(1+\lambda_n)\cos\left(\frac{\pi}{2}r^2\right)\right]V_n=-\frac{q}{Sr}\varepsilon^{-1/q}r_1^{(1+1/q)}U_r\frac{\mathrm{d}V_n}{\mathrm{d}r_1} \tag{30}$$

which shows that, when $\varepsilon^{1-2/q}=1$ or $q=2$, the first two terms representing viscous and inertial forces will be of the same order of magnitude where U_r vanishes.

Transition Scale

The scaling analysis also shows that there exists a buffer region adjacent to the centerline region where viscous and mean flow convection forces are in balance. When the radial mean velocity component is no more negligible, a value of $q=1$ will characterize this layer of undetermined size. In this buffer region that is sufficiently removed from the solid surface, the same scaling analysis shows that mean flow convection and viscous diffusion become of the same order. Blowing effects become as important as viscous diffusion. To expand the transition region, a less intense stretching of the scale is required by comparison to the centerline scale. Introducing a magnified scale of a form that is similar to the centerline scale, a balance between convection and viscous diffusion can be achieved in Eq. (26):

$$q^2\varepsilon^{1-2/q}\left(r_1^{2(1+1/q)}\frac{\mathrm{d}^2V_n}{\mathrm{d}r_1^2}+r_1^{(1+2/q)}\frac{\mathrm{d}V_n}{\mathrm{d}r_1}\right)+\frac{q}{Sr}\varepsilon^{-1/q}r_1^{(1+1/q)}U_r\frac{\mathrm{d}V_n}{\mathrm{d}r_1}=-\left[i-\frac{\pi}{Sr}(1+\lambda_n)\cos\left(\frac{\pi}{2}r^2\right)\right]V_n \tag{31}$$

where it can be easily seen that convective and viscous force terms will be of the same order of magnitude when $\varepsilon^{1-2/q}=\varepsilon^{-1/q}$ or $q=1$.

Unmodified Base Scale

In a region extending from the edge of the buffer region to the edge of the near-wall region, all three physical phenomena, namely, convection, diffusion, and inertia, need to be included to account for the resulting fluid motion. Mathematically, all of the terms in Eq. (26) must be retained. The base scale at which level all three physical phenomena are in balance will correspond to the spatial coordinate itself. The viscous term is no more negligible because, in this region, velocity gradients vary rapidly in the radial direction due to a reduction in the spatial wavelength. Hence, for $r_0 = r$, Eq. (26) is unaltered.

Note that, from the preceding scaling analysis, viscous forces appear to play a significant role in a region that is blown off the wall by the strong radial mean flow component. Because of radial injection, the traditionally thin and highly viscous region, which usually occurs at the wall in no-injection flowfields, takes the form here of a free unlocalized shear layer separating the rotational from the irrotational flow. This result is very similar to that of the blowhard problem and is well described by Cole and Aroesty,[19] who analyzed a steady flow with sidewall injection.

Composite Scale

Because the problem involves events occurring at three different scales, other than the base scale, a strict multiple-scales technique will require utilizing four scales and integrating three times up to the third term for a one-term solution to be feasible.[15] It can be easily shown that, in this particular problem, for a complete analytical expression to be possible the method of multiple scales will have to be limited to two scales only. Hence, a solution that is uniformly valid in the entire range of interest is reachable if a composite scale can be devised to provide the same geometric description that is available from the near-wall, transition, and centerline scales in their regions of applicability. Therefore, a composite scale that is valid in the entire region extending from the centerline to the wall must be constructed such that

$$s(r)=\frac{(1-r)}{r^q}\approx\begin{cases}1-r & (\text{as } r\to 1)\\ 1/r & (\text{in the buffer region})\\ 1/r^2 & (\text{as } r\to 0)\end{cases} \tag{32}$$

If the stretching exponent[13,14] q is defined to be a spatial function that approaches 0 in the neighborhood of $r=1$, approaches 1 in the buffer region, and approaches 2 at the centerline, then a controllable agreement with the exact solution to Eq. (26) can be achieved everywhere ($0 \le r \le 1$). It is found that using a variable stretching exponent that is dependent on the geometry involved, such as $q(r) = q(1-r)^g$, minimizes the error between the numeric and multiple-scales solutions. Fortunately, the parameters involved in the variable stretching exponent $q(r)$ can be determined to any degree of desired precision. For instance, the error between the numerical and analytical predictions is found to be less than 1% when $q = g = \frac{3}{2}$.

Composite-Scale Solution

One major advantage of the present method is its accuracy; using a combination of two scales, the zeroth-order term in this solution will have the same order as a two-term solution using regular perturbations.[15] Another advantage is its compactness. Unlike regular perturbations where the solution to the first order is a linear combination of two terms, the first-order solution here is only one term that contains information from both the zeroth- and first-order perturbed equations as well. This so-called derivative-expansion method consists of expanding the derivatives, as well as the dependent variables in powers of the small parameter ε, to attain uniformly valid expansions.[15] In what follows, a generalized solution will be derived that is applicable to any characteristic scale. From the generalized expression, solutions corresponding to any characteristic scale can be readily obtained.

Generalized Two-Term Expansion

The two scales to be used in Eq. (26) are 1) the base $r_0 \equiv r$ and 2) the modified scale $r_1 \equiv \varepsilon s(r) \equiv \varepsilon s(r_0)$, written in the most general form for any scale function corresponding to a transformation of the coordinate in the near-wall, transition, or centerline regions. The value of the modified scale can, thus, be any one of

$$s(r_0)=\begin{cases}1-r_0 & (\text{near wall})\\ r_0^{-q} & (\text{near center})\\ (1-r_0)r_0^{-q(r_0)} & (\text{composite})\end{cases} \tag{33}$$

Using the chain rule for differentiation and carrying as many terms as will be needed to retain a final order of ε^2, the derivatives can be expanded as follows:

$$\frac{\mathrm{d}}{\mathrm{d}r}=\frac{\partial}{\partial r_0}+\varepsilon\frac{\mathrm{d}s}{\mathrm{d}r_0}\frac{\partial}{\partial r_1}+\mathcal{O}(\varepsilon^2),\qquad \frac{\mathrm{d}^2}{\mathrm{d}r^2}=\frac{\partial^2}{\partial r_0^2}+\mathcal{O}(\varepsilon) \tag{34}$$

After substitution of Eq. (34) into Eq. (26), the latter is transformed into a partial differential equation (PDE) that is function of two independent coordinates r_0 and r_1:

$$\varepsilon\left(\frac{\partial^2V_n}{\partial r_0^2}+\frac{1}{r_0}\frac{\partial V_n}{\partial r_0}\right)-\frac{U_r}{Sr}\frac{\partial V_n}{\partial r_0}-\varepsilon\frac{U_r}{Sr}\frac{\mathrm{d}s}{\mathrm{d}r_0}\frac{\partial V_n}{\partial r_1}+\left[i-\frac{\pi}{Sr}(1+\lambda_n)\cos\left(\frac{\pi}{2}r_0^2\right)\right]V_n+\mathcal{O}(\varepsilon^2)=0 \tag{35}$$

Following the multiple-scales procedure, the velocity is now written using a two-term expansion that is a function of the two independent scales:

$$V_n(r_0, r_1) = V_n^{(0)}(r_0, r_1) + \varepsilon V_n^{(1)}(r_0, r_1) + \mathcal{O}(\varepsilon^2) \tag{36}$$

Substituting the perturbed two-term expansion given by Eq. (36) into Eq. (35), rearranging, and collecting terms of order ε^0 and ε^1, two first-order coupled PDEs must be satisfied for any value of ε. These are

$$-\frac{U_r}{Sr}\frac{\partial V_n^{(0)}}{\partial r_0} + \left[i - \frac{\pi}{Sr}(1+\lambda_n)\cos\left(\frac{\pi}{2}r_0^2\right)\right]V_n^{(0)} = 0 \tag{37}$$

$$-\frac{U_r}{Sr}\frac{\partial V_n^{(1)}}{\partial r_0} + \left[i - \frac{\pi}{Sr}(1+\lambda_n)\cos\left(\frac{\pi}{2}r_0^2\right)\right]V_n^{(1)} = \frac{U_r}{Sr}\frac{\mathrm{d}s}{\mathrm{d}r_0}\frac{\partial^2 V_n^{(0)}}{\partial r_1} - \frac{\partial^2 V_n^{(0)}}{\partial r_0^2} - \frac{1}{r_0}\frac{\partial V_n^{(0)}}{\partial r_0} \tag{38}$$

The boundary conditions given by Eqs. (27) and (28) for the velocity V_n can be translated to the first perturbation term $V_n^{(0)}$, which must satisfy the same condition as V_n in the limit when ϵ approaches zero, as can be clearly seen from Eq. (36). The resulting boundary conditions that must be satisfied by $V_n^{(0)}$ are as follows.

No slip:

$$V_n^{(0)}(r_0 = 1) = 1 \tag{39}$$

Axial symmetry:

$$\frac{\partial V_n^{(0)}}{\partial r_0}(r_0 = 0) = 0 \tag{40}$$

Nonsecular Integration

The next step in the multiple-scales technique is to integrate Eq. (37), which is solely a function of the first scale, for the zeroth-term solution. The integration constant that must be a function of the second scale will have to be determined after substitution into Eq. (38) and examination of the possibility of removing secular terms, which if retained will cause the solution to become nonuniformly valid. Complete closure is later accomplished by applying the boundary conditions.

First Integration

Equation (37) is a homogeneous first-order PDE with a variable coefficient that is solely a function of r_0. Using $\theta_0 = \pi r_0^2/2$, direct integration yields

$$V_n^{(0)} = C_1(r_1)\exp[(1+\lambda_n)\,\ell_\nu \sin\theta_0 - i(Sr/\pi)\,\ell_\nu \tan(\theta_0/2)] \tag{41}$$

Because integration is carried out with respect to r_0 only, the constant of integration C_1 can, in general, be a function of r_1 as well.

Removing Secular Terms

First and second partial derivatives of $V_n^{(0)}$ are

$$\frac{\partial V_n^{(0)}}{\partial r_0} = C_1(r_1)[-iSrr_0\csc\theta_0 + \pi(1+\lambda_n)r_0\cot\theta_0] \times \exp\left[(1+\lambda_n)\,\ell_\nu\sin\theta_0 - i\frac{Sr}{\pi}\,\ell_\nu\tan\frac{\theta_0}{2}\right] \tag{42}$$

$$\frac{\partial V_n^{(0)}}{\partial r_1} = \frac{\mathrm{d}C_1}{\mathrm{d}r_1}\exp\left[(1+\lambda_n)\,\ell_\nu\sin\theta_0 - \frac{iSr}{\pi}\,\ell_\nu\tan\frac{\theta_0}{2}\right] \tag{43}$$

$$\frac{\partial^2 V_n^{(0)}}{\partial r_0^2} = \{-Sr^2r_0^2\csc^2\theta_0 + \pi(1+\lambda_n)\cot\theta_0 - iSr\csc\theta_0[1+\pi(1+2\lambda_n)r_0^2\cot\theta_0] + \pi^2(1+\lambda_n)r_0^2(\lambda_n\cot^2\theta_0 - 1)\}V_n^{(0)} \tag{44}$$

Now by substituting Eqs. (42–44) into Eq. (38), the right-hand side becomes a source of secular terms. To remove secular terms that cause the solution to degenerate, a mathematical requirement that satisfies the symmetry condition, given by Eq. (40), is that the right-hand side be zero; this implies that

$$-\frac{U_r}{Sr}\frac{\partial V_n^{(1)}}{\partial r_0} + \left[i - \frac{\pi}{Sr}(1+\lambda_n)\cos\theta_0\right]V_n^{(1)} = \left[\frac{U_r}{Sr}\frac{\mathrm{d}s}{\mathrm{d}r_0}\frac{\mathrm{d}C_1}{\mathrm{d}r_1} - C_1\{-Sr^2r_0^2\csc^2\theta_0 + 2\pi(1+\lambda_n)\cot\theta_0 + \pi^2(1+\lambda_n) \times r_0^2(\lambda_n\cot^2\theta_0 - 1) - iSr\csc\theta_0[2+\pi(1+2\lambda_n)r_0^2\cot\theta_0]\}\right] \times \exp\left[(1+\lambda_n)\,\ell_\nu\sin\theta_0 - i\frac{Sr}{\pi}\,\ell_\nu\tan\frac{\theta_0}{2}\right] \equiv 0 \tag{45}$$

yielding a first-order ODE that can be solved for C_1:

$$\frac{\mathrm{d}C_1(r_1)}{\mathrm{d}r_1} + C_1(r_1)Sr\{-Sr^2r_0^2\csc^2\theta_0 + \pi^2(1+\lambda_n) \times r_0^2(\lambda_n\cot^2\theta_0 - 1) - iSr\csc\theta_0[2+\pi(1+2\lambda_n)r_0^2\cot\theta_0] + 2\pi(1+\lambda_n)\cot\theta_0\}r\csc\theta_0\left(\frac{\mathrm{d}s}{\mathrm{d}r_0}\right)^{-1} = 0 \tag{46}$$

Second Integration

Integration of Eq. (46), subject to satisfaction of the no-slip condition given by Eq. (39), allows the complete determination of C_1. Using $\theta = \pi r^2/2$, the result is

$$C_1(r) = \exp\{\xi[r^3\csc^3\theta\eta(r) - \eta(1)] - (\xi/Sr^2)\pi(1+\lambda_n) \times \{r\csc\theta\eta(r)[2\cot\theta + \pi r^2(\lambda_n\cot^2\theta - 1)] + \pi\eta(1)\} + \frac{i\pi\xi}{Sr}\{r\csc^2\theta\eta(r)[2+\pi r^2\cot\theta(1+2\lambda_n)] - 2\eta(1)\}\} \tag{47}$$

The effective scale function η that appears in the solution is the ratio of the scale and its first derivative:

$$\eta(r) = s(r)\left(\frac{\mathrm{d}s}{\mathrm{d}r}\right)^{-1} \tag{48}$$

From Eq. (36), V_n can be written to the order of ε^2, for any effective scale η and any eigenvalue λ_n. This is typically the case because information from both first- and second-perturbation levels are included in the first term of the multiple-scales expansion for V_n:

$$V_n(r) = (\sin\theta)^{(1+\lambda_n)}\exp\{\xi[r^3\csc^3\theta\eta(r) - \eta(1)] + i\pi(\xi/Sr)\{2r\csc^2\theta\eta(r)[1+\theta\cot\theta(1+2\lambda_n)] - 2\eta(1)\}) \times (-\xi/Sr^2)\{2r\csc\theta\eta(r)[\cot\theta + \theta(\lambda_n\cot^2\theta - 1)] + \pi\eta(1)\} \times \pi(1+\lambda_n) - i(Sr/\pi)\,\ell_\nu\tan(\theta/2) \tag{49}$$

Uniformly Valid Solution

In this case, for $y = 1 - r$, $s(r) = yr^{-qy^g}$, we get

$$\eta(r) = -y[1 + qy^g(yr^{-1} - g\,\ell_\nu r)]^{-1}, \qquad q = g = \tfrac{3}{2} \tag{50}$$

$$V_n(r) = \sin^{1+\lambda_n}\theta\exp\{\xi r^3\csc^3\theta\eta(r) - (iSr/\pi)\,\ell_\nu\tan(\theta/2) - (2\pi\xi/Sr^2)(1+\lambda_n)r\csc\theta\eta(r)[\cot\theta + \theta(\lambda_n\cot^2\theta - 1)] + 2i\pi(\xi/Sr)r\csc^2\theta\eta(r)[1+\theta\cot\theta(1+2\lambda_n)]\} \tag{51}$$

Description of the Radially Dependent Velocity

The radially dependent velocity function corresponding to the multiple-scales solution given by Eq. (51) is virtually indistinguishable from the numeric solution to Eq. (26). The function $V_n(r)$ is best described as an upward-traveling harmonic wave with an amplitude that suffers an exponential damping with increasing distance from the wall. This damping is found to depend on the penetration number S_p or ξ^{-1}.

Rotational Flowfield

Substituting Eq. (51) into Eq. (25), the result is

$$\tilde{u}_z(r,z) = -\frac{\varepsilon_w}{\gamma} i \sum_{n=0}^{\infty} \frac{(-1)^n (k_m z)^{2n+1}}{(2n+1)!} (\sin\theta)^{(2n+2)}$$
$$\times \exp\left\{ \xi r^3 \csc^3\theta \eta(r) - i\frac{Sr}{\pi} \ell_\nu \tan\frac{\theta}{2} \right.$$
$$\times \frac{-2\pi\xi}{Sr^2}(1+\lambda_n) r \csc\theta \eta(r)\left[\cot\theta + \theta(\lambda_n \cot^2\theta - 1)\right]$$
$$\left. + 2i\pi \frac{\xi}{Sr} r \csc^2\theta \eta(r)[1 + \theta\cot\theta(1+2\lambda_n)] \right\} \quad (52)$$

Infinite Series Solution

The rotational component $\tilde{u}_z$ can now be written in terms of an infinite series, including all of the terms that originate from the full momentum equation (10). Regrouping and inserting elementary trigonometric identities, the solution can be written in a form that clearly displays the dominating terms and the smaller terms of order Sr^{-2}:

$$\tilde{u}_z(r,z,t) = -\frac{\varepsilon_w}{\gamma} i \sin\theta \sum_{n=0}^{\infty} \frac{(-1)^n (k_m z \sin\theta)^{2n+1}}{(2n+1)!}$$
$$\times \exp\left(-ik_m t - i\frac{Sr}{\pi} \ell_\nu \tan\frac{\theta}{2} + \xi\eta r^3 \csc^3\theta \left\{ 1 - \frac{\pi^2}{Sr^2} \right.\right.$$
$$\left.\times (1+\lambda_n)\left[\cos 2\theta + \frac{\sin 2\theta}{2\theta} + (\lambda_n - 1)\cos^2\theta \right]\right\}$$
$$\left. + 2i\pi \frac{\xi}{Sr} \eta r \csc^2\theta[1 + \theta\cot\theta(1+2\lambda_n)] \right) \quad (53)$$

Fortunately, this is a rapidly converging series that requires only two terms to yield results that compare extremely well with the solution corresponding to a very large number of terms.

Closed-Form Solution

Analyzing carefully the preceding infinite expression shows that it can be written in a closed form by ignoring terms that are much smaller than the order of precision associated with the infinite series itself. The result is an alternative closed-form expression that can be written in a compact form in terms of a spatial damping function ζ and a spatial phase angle Φ. A practically equivalent expression to Eq. (53) is, hence,

$$\tilde{u}_z = -(\varepsilon_w/\gamma) i \sin\theta \sin(k_m z \sin\theta) \exp[\zeta - i(k_m t + \Phi)] \quad (54)$$

where zeroth- and first-order terms in ζ and Φ are

$$\zeta = \zeta_0 + \zeta_1, \qquad \Phi = \Phi_0 + \Phi_1 \quad (55)$$

$$\zeta_0(r) = \xi\eta(r) r^3 \csc^3\theta, \qquad \Phi_0(r) = (Sr/\pi)\,\ell_\nu \tan(\theta/2) \quad (56)$$

$$\zeta_1(r) = -\frac{2\pi^2}{Sr^2} \xi\eta(r) r^3 \csc^3\theta \left(\cos 2\theta + \frac{\sin 2\theta}{2\theta} \right) \quad (57)$$

$$\Phi_1(r) = -2\pi(\xi/Sr)\eta(r) r \csc^2\theta(1 + 3\theta\cot\theta) \quad (58)$$

Simplified Solution

The closed-form expression can be further simplified by neglecting terms of order Sr^{-2} and higher. As one would expect, because Sr^{-2} is smaller than M_b, no loss in accuracy is incurred by so doing. The resulting simple expression agrees with both numerical and infinite series results with a margin of error that is smaller than M_b. Because there is no need to be more accurate than the governing momentum equation itself, which neglects $\tilde{u}_r$ of order M_b, a short practical expression can now be offered by retaining the zeroth-order terms and dropping smaller terms given by Eqs. (57) and (58). The result is a simple yet accurate form:

$$\tilde{u}_z = -\frac{\varepsilon_w}{\gamma} i \sin\theta \sin(k_m z \sin\theta) \exp\left(\frac{\xi\eta r^3}{\sin^3\theta} - i\frac{Sr}{\pi} \ell_\nu \tan\frac{\theta}{2} - ik_m t \right) \quad (59)$$

Other than its simplicity and remarkable agreement with the infinite series solution [Eq. (53)], the advantage of Eq. (59) is that it only contains the important terms that affect the solution. It can be easily shown that 1) retaining the axial convection of unsteady vorticity leads to the axially dependent sinusoidal function; 2) retaining radial convection leads to the term involving the Strouhal number, which controls the spatial wavelength; and 3) retaining viscous diffusion leads to the rotational wave damping term controlled by the penetration number.

Radial Velocity Component

The radial component of the rotational velocity can be derived analytically from the continuity equation, which suggests first assuming an ansatz of the form[18]

$$\tilde{u}_r = (\varepsilon_w/\gamma)[F(r)/r]\cos(k_m z \sin\theta)\exp[\zeta - i(k_m t + \Phi)] \quad (60)$$

Substituting Eq. (60) into the continuity equation and balancing the highest-order terms, one can deduce the spatial function $F(r)$:

$$\frac{1}{r}\frac{\partial(r\tilde{u}_r)}{\partial r}\bigg|_{\text{largest}} = -\frac{\partial \tilde{u}_z}{\partial z} \Rightarrow F(r) = -M_b \sin^3\theta \quad (61)$$

Consequently, the radial component is determined:

$$\tilde{u}_r = -(\varepsilon_w/\gamma)(M_b/r)\sin^3\theta\cos(k_m z\sin\theta)\exp[\zeta - i(k_m t + \Phi)] \quad (62)$$

This reassuring result justifies the assumption of $\tilde{u}_r/\tilde{u}_z = \mathcal{O}(M_b)$ in Eq. (9). From Eq. (2), $u_r^{(1)} = \tilde{u}_r$ also. The fact that the radial oscillatory component does not vanish in the vicinity of the wall constitutes a significant departure from one-dimensional acoustic model predictions that do not account for radial fluctuations. Inclusion of this term in combustion stability assessments is expected to improve the accuracy of existing predictions. Exploring resulting implications is beyond the scope of this paper and will be addressed in subsequent work.

Total Time-Dependent Velocity

The total unsteady axial velocity can now be constructed by juxtaposition of the rotational [Eq. (54)] and irrotational [Eq. (46)] parts in Eq. (2). The result is

$$u_z^{(1)} = (\varepsilon_w/\gamma)[\sin\bar{z}\sin\bar{t} - \sin\theta\sin(\bar{z}\sin\theta)e^{\zeta}\sin(\bar{t} + \Phi)] \quad (63)$$

where $\bar{z} = k_m z$ and $\bar{t} = k_m t$.

This result has been tested for the entire range of possible parameters[14] and has been found to match very closely both the numerical solution to the governing momentum equation (using a fourth-order method with a truncation error of 10^{-20}) and Flandro's latest result.[18] The results are so close that, for comparison purposes, when curves are overlayed that correspond to Eq. (63), the numerical solution, and Flandro's solution,[18] only one curve is visually discerned. The ability of this multiple-scales solution and of Flandro's regular perturbation solution to match the numerical solution is quite remarkable. For illustration purposes, Eq. (63) is evaluated for three cardinal cases spanning the range of rocket motors (given in Ref. 17) for typical tactical rocket, small research rocket, and large Shuttle rocket booster. The error between analytical and computational predictions appears only in the third or fourth significant digit, causing a relative error of less than 1%, which is difficult to discern visually. This agreement is found to get even better at higher modes.

A graphical representation of Culick's[12] steady flowfield along with the total unsteady velocity derived here is given in Figs. 1 and 2, at several discrete axial locations and at times of maximum amplitude for the three cardinal cases at the fundamental oscillation mode. Indiscernible from the regular perturbation results obtained by Flandro[18] using a totally different formulation, or from the numerical solution to the momentum equation, these profiles (in Fig. 2) show an asymmetric behavior with respect to the chamber midpoint and a Richardson's velocity overshoot[20] near the wall that is not accounted for in the plain one-dimensional acoustic model. More flow details are given in Figs. 3–8 corresponding to the forward and

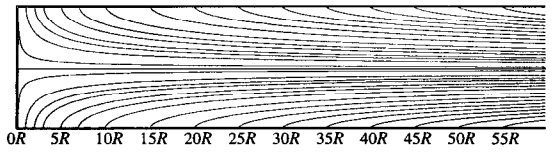

Fig. 1 Culick's[12] steady flow streamlines.

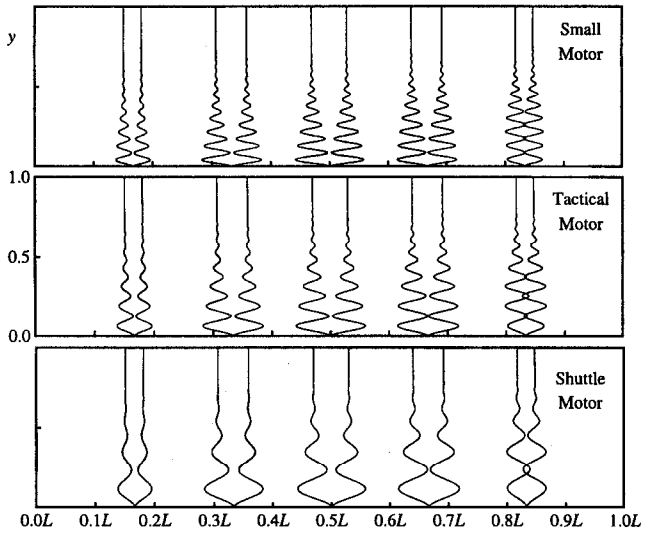

Fig. 2 Time-dependent velocity patterns.

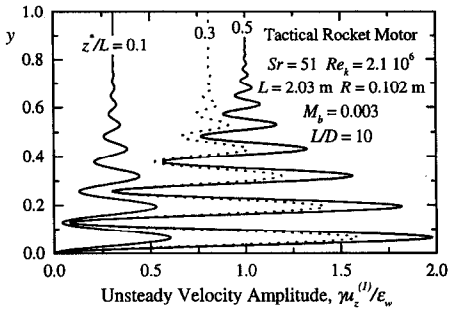

Fig. 3 Unsteady velocity amplitude (fore half).

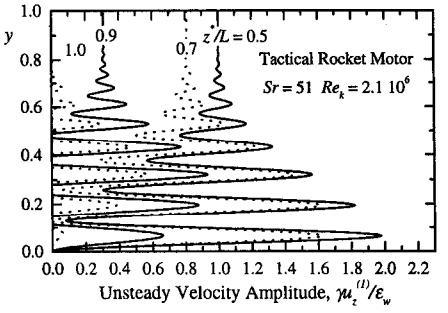

Fig. 4 Unsteady velocity amplitude (aft half).

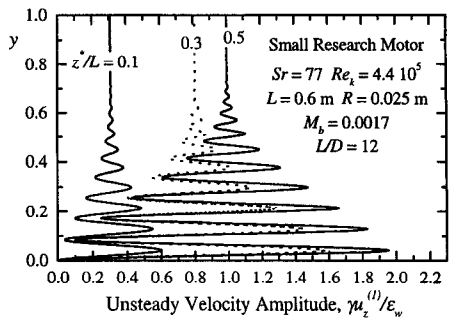

Fig. 5 Unsteady velocity amplitude (fore half).

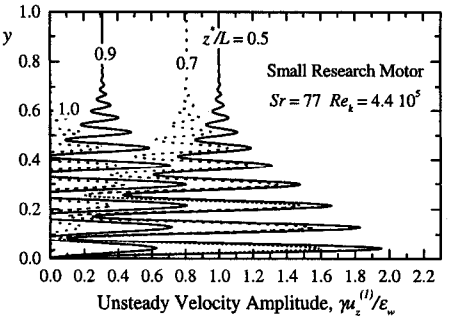

Fig. 6 Unsteady velocity amplitude (aft half).

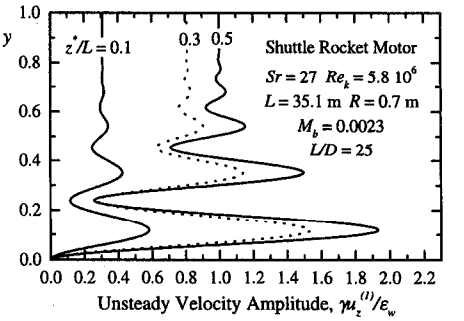

Fig. 7 Unsteady velocity amplitude (fore half).

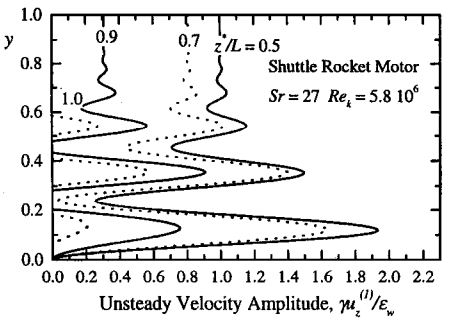

Fig. 8 Unsteady velocity amplitude (aft half).

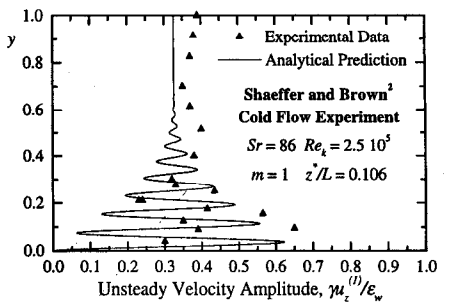

Fig. 9 Comparison to cold flow data at $z^*/L = 0.106$.

aft halves of each particular motor. Note that the rotational velocity amplitude is larger in the aft half by comparison to its corresponding value at a point that is equidistant from the chamber midpoint in the forward half. This asymmetry is to be expected due to the added rotational effects that accompany the downstream convection of unsteady vorticity by Culick's axial mean flow component.[12] The previously reported flowfield solution by Majdalani and Van Moorhem[14] was not capable of accounting for these enhanced vortical effects because it did not incorporate the dependence of the rotational field on the axial location within the chamber due to the downstream convection of vorticity. Contrary to one-dimensional predictions that do not include axial variations in the rotational field, the unsteady velocity amplitude is not zero everywhere at $z^* = L$. Also, note that for higher oscillation frequencies corresponding to shorter rocket motors, the rotational wavelength is decreased, being

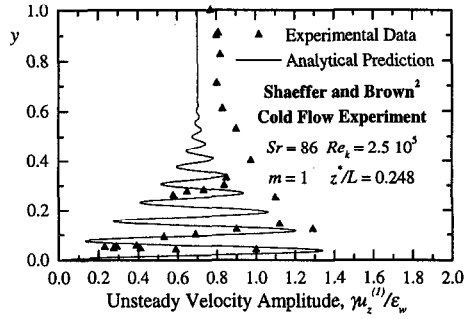

Fig. 10 Comparison to cold flow data at $z^*/L = 0.248$.

an inverse function of the Strouhal number. Comparison of current analytical predictions to cold flow data taken from an elegant experiment by Shaeffer and Brown[2] is further reassuring. For example, Figs. 9 and 10 reflect a fair agreement with theory, well within experimental uncertainty, at two axial locations in the chamber.

Concluding Remarks

Flandro's latest model[18] results from a careful application of perturbation theory. The methodology that is employed is analogous to Culick's approach[12] to the steady flow. The results are equally accurate for the time-dependent field. They match both numerical and analytical predictions presented here using totally different procedures.

The multiple-scales formulation presented is a successful alternative to matched asymptotic expansions that fail to yield a uniformly valid solution to a singular perturbation problem. This is accomplished using an innovative technique that consists of matching the scales rather than the asymptotic solutions in a boundary-layer problem. In this approach, all of the terms in the momentum equation are retained without neglecting any of the smaller terms in the process of integration except for the radial velocity component that is of order M_b and that has been totally ignored in all previous analytical models. No approximation is applied to the boundary condition such as found necessary in Flandro's approach.[18] The rotational velocity is derived by direct integration of the momentum equation. The analytical expression that is derived is theoretically accurate to the order of Re_k^{-2}. However, due to the need to match three different scales that arise in the problem with a single composite scale, the final outcome is a solution that is as accurate as the matching procedure. Fortunately, the matching process can be done very precisely to the point that the composite scale solution and the full numerical solution are indistinguishable in the entire range of the physical parameters. The main advantage of this technique over previous models is that it incorporates all of the effects that characterize the problem in a compact expression where the key elements that control the solution are clearly seen. The dependence of the solution on the penetration number, the mode number, and the axial location is clearly depicted from inspection of the solution. Another advantage of this method is that the inviscid formulation can be readily produced from the resulting solution by setting the viscous parameter ξ to be zero. In the previous model,[18] the complete viscous solution relied on the inviscid formulation, which had to be derived beforehand.[17]

Finally, the analytical solution presented here corresponds to a laminar field in a cold flow environment. It neither accounts for turbulence nor incorporates the effect of coupling with the flame zone. Its simplicity holds the advantage of permitting further investigations of analytical models for turbulence, particle damping, flow reversal, and coupling with combustion near the burning surface. Details of subsequent implications on combustion stability will be deferred to another paper and will be reported in our forthcoming work.

Acknowledgments

The authors wish to thank the editor and anonymous referees for their constructive comments. They also wish to thank Gary A. Flandro for his valuable suggestions.

References

[1]Culick, F. E. C., and Yang, V., "Stability Predictions in Rockets," *Nonsteady Burning and Combustion Stability of Solid Propellants*, Vol. 143, Progress in Astronautics and Aeronautics, AIAA, Washington, DC, 1992, pp. 719–799.

[2]Shaeffer, C. W., and Brown, R. S., "Oscillatory Internal Flow Studies," Chemical Systems Div., Rept. 2060 FR, United Technologies, San Jose, CA, Aug. 1992.

[3]Vuillot, F., and Avalon, G., "Acoustic Boundary Layer in Large Solid Propellant Rocket Motors Using Navier–Stokes Equations," *Journal of Propulsion and Power*, Vol. 7, No. 2, 1991, pp. 231–239.

[4]Smith, T. M., Roach, R. L., and Flandro, G. A., "Numerical Study of the Unsteady Flow in a Simulated Rocket Motor," AIAA Paper 93-0112, Jan. 1993.

[5]Flandro, G. A., and Roach, R. L., "Effects of Vorticity Production on Acoustic Waves in a Solid Propellant Rocket," AFOSR Final Rept., AFOSR-90-0159, Air Force Office of Scientific Research, Bolling AFB, DC, Oct. 1992.

[6]Sabnis, J. S., Giebeling, H. J., and McDonald, H., "Navier–Stokes Analysis of Solid Propellant Rocket Motor Internal Flows," *Journal of Propulsion and Power*, Vol. 5, No. 6, 1989, pp. 657–664.

[7]Zhao, Q., and Kassoy, D. R., "The Generation and Evolution of Unsteady Vorticity in a Model of a Solid Rocket Engine Chamber," AIAA Paper 94-0779, Jan. 1994.

[8]Kirkkopru, K., Kassoy, D. R., and Zhao, Q., "Unsteady Vorticity Generation and Evolution in a Model of a Solid Rocket Motor: Sidewall Mass Addition Transients," AIAA Paper 95-0603, Jan. 1995.

[9]Nickerson, G. R., Coats, D. E., and Hermsen, R. W., "A Computer Program for the Prediction of Solid Propellant Rocket Motor Performance," Air Force Rocket Propulsion Lab., Interim TR, AFRPL-TR-80-34, Air Force Systems Command, Edwards AFB, CA, Oct. 1981.

[10]Flandro, G. A., "Solid Propellant Acoustic Admittance Corrections," *Journal of Sound and Vibration*, Vol. 36, No. 3, 1974, pp. 297–312.

[11]Flandro, G. A., "Effects of Vorticity Transport on Axial Acoustic Waves in a Solid Propellant Rocket Chamber," *Combustion Instabilities Driven by Thermo-Chemical Acoustic Sources*, NCA Vol. 4, HTD Vol. 128, American Society of Mechanical Engineers, New York, 1989.

[12]Culick, F. E. C., "Rotational Axisymmetric Mean Flow and Damping of Acoustic Waves in a Solid Propellant Rocket," *AIAA Journal*, Vol. 4, No. 8, 1966, pp. 1462–1464.

[13]Majdalani, J., and Van Moorhem, W. K., "The Unsteady Boundary Layer in Solid Rocket Motors," AIAA Paper 95-2731, July 1995.

[14]Majdalani, J., and Van Moorhem, W. K., "A Multiple-Scales Solution to the Acoustic Boundary Layer in Solid Rocket Motors," *Journal of Propulsion and Power*, Vol. 13, No. 2, 1997, pp. 186–193.

[15]Nayfeh, A., *Perturbation Methods*, Wiley, New York, 1973, pp. 228–303.

[16]Van Dyke, M., *Perturbation Methods in Fluid Mechanics*, Parabolic, Stanford, CA, 1975, pp. 195–213.

[17]Flandro, G. A., "Effects of Vorticity on Rocket Combustion Stability," *Journal of Propulsion and Power*, Vol. 11, No. 4, 1995, pp. 607–625.

[18]Flandro, G. A., "On Flow Turning," AIAA Paper 95-2730, July 1995.

[19]Cole, J. D., and Aroesty, J., "The Blowhard Problem-Inviscid Flows with Surface Injection," *International Journal of Heat and Mass Transfer*, Vol. 11, No. 7, 1968, pp. 1167–1183.

[20]Richardson, E. G., and Tyler, E., "The Transverse Velocity Gradient Near the Mouths of Pipes in Which an Alternating or Continuous Flow of Air Is Established," *Proceedings of the Physical Society, London*, Vol. 42, Pt. 1, 1929, pp. 1–15.

G. M. Faeth
Associate Editor